

## **Analysis the Effect of Different Fluid Temperature and Pressure to The Flow and Pipe Structure Longevity for Plant Pipeline**

**Akif Akmal Hakimi Sahizan<sup>1</sup>, Zuliazura Mohd Salleh<sup>1\*</sup>**

<sup>1</sup>Department of Mechanical Engineering Technology, Faculty of Engineering Technology, Universiti Tun Hussein Onn Malaysia, 84600 Pagoh, Johor, MALAYSIA

\*Corresponding Author Designation

DOI: <https://doi.org/10.30880/peat.2022.03.01.087>

Received 17 January 2022; Accepted 11 April 2022; Available online 25 June 2022

**Abstract:** Pipes are widely used in many fields, such as construction sites, homes, and many fields including power plants. Under some conditions, stress generated by the inlet pressure of the desired fluid in the pipeline might cause stress distribution, which can lead to material crack and fracture failure. The piping system of a power plant can be classified as one of the key components of the power plant because it performs the task of transferring fluid from one process to another. The purpose of this study is to analyze the influence of different fluid temperatures (27 °C and 77 °C) and three different pressures inlet (153 kPa, 200 kPa, and 250 kPa) to the pipe flow behavior and pipe structural performance. The layout 3D model for the pipeline is based on the pipeline used at the UTHM Biodiesel Plant starting from the esterification process until the trans-esterification process. The result of the study is to identify the location in the pipe that handles the highest stress distribution. ANSYS 19.2 software was used to conduct the simulation to determine the velocity, pressure, and stress distribution. The result from the simulation shows that at pressure inlet 250 kPa, the highest stress distribution located at fitting 10 with the value of stress is 3.045 MPa.

**Keywords:** Flow in Pipe, ANSYS Simulation, Stress Distribution, Fluid-structure Interaction

### **1. Introduction**

Biodiesel is a sustainable and environmentally beneficial substitute diesel fuel for diesel engines [1]–[3]. It can be made from edible and inedible vegetables, animal fat, and waste cooking oils, and it is non-toxic, biodegradable, and ecologically sustainable [4], [5]. The current global biodiesel standards are mostly based on a biodiesel–diesel blend. Blends of biodiesel–diesel are marked as "B" followed by a number representing the blending volumetric percentage of biodiesel, according to [6]. For example, B100 indicates 100 percent of pure biodiesel, whereas B20 represents a mixture of 20 percent

---

\*Corresponding author: [zulia@uthm.edu.my](mailto:zulia@uthm.edu.my)

2022 UTHM Publisher. All rights reserved.

[publisher.uthm.edu.my/periodicals/index.php/peat](http://publisher.uthm.edu.my/periodicals/index.php/peat)

biodiesel and 80 percent petroleum fuel. The study is also conducted using simulation analysis to determine flow behavior and structural performance, as well as possible risks in the pipeline's operation.

The study has been conducted at UTHM Biodiesel Plant while using its pipeline system as a reference to 3D pipeline modeling. The result can be used to predict the location in the pipe that handles the highest stress distribution. In this study, the pipeline used at the UTHM Biodiesel Plant is focused on starting from the esterification process until the transesterification process. The analysis has done of effect from three different inlet pressures and two different fluid temperatures to flow behavior and structure performance of the pipeline.

### 1.1 Process of biodiesel

The research was carried out from esterification to trans-esterification because biodiesel production began at that phase. Esterification is a chemical process that uses acid to make fatty acid alkyl ester and water ( $H_2O$ ) from free fatty acid (FFA) and alcohol [7]. The difference between esterification and transesterification is that an ester is produced by esterification, whereas an ester is a reactant in transesterification. Common vegetable oils and animal fats are trihydric alcohol glycerides esters of saturated and unsaturated monocarboxylic acids [8], [9]. Triglycerides are esters that can react with alcohol in the presence of a catalyst[10]. The presence of a catalyst (a strong acid or basic) however, enhances the conversion. This method has been frequently utilized to decrease triglyceride viscosity. The type of the triglycerides can, in effect, impact the biodiesel's properties.

### 1.2 Introduction to design and pipeline system

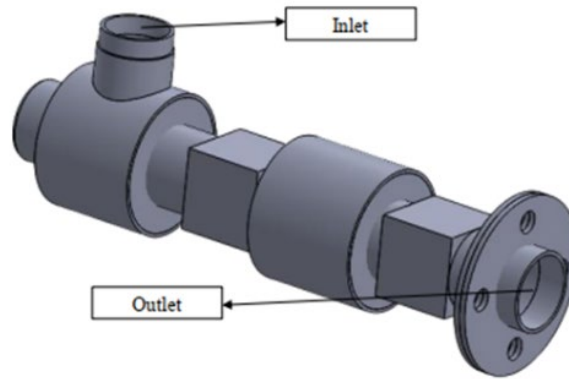
The piping system consists of many interconnected piping components to form a complex network [11]–[13]. Pipelines serve a significant purpose in biodiesel processing. The pipeline system's initial design is created on the basis needs for moving fluid from one location to another[14]. The transmission fluid type, permitted pressure drop or energy loss, needed speed, space constraints, process requirements, stress analysis, fluid temperature, and other criteria are all factors that go into the detailed design. Since pipelines play a major role, it is important to always keep good maintenance. The structure of a pipeline system can be split into repairable and non-repairable units in terms of maintenance [15]. A repairable structure is one that is fixed to restore its functionality rather than being scrapped after each failure[16]. The pipeline system must be maintained on a periodic basis to maintain structural integrity and improve service levels[11].

## 2. Methodology

The geometry model of the pipe is drawn using Solidwork. Simulation methods using fluid fluent and static structural from Ansys 19.2 were utilized in this study to represent the Fluid-structure Interaction (FSI). The three different pressure and two different temperatures have been input into the simulation method to be analyzed.

### 2.1 3D modelling

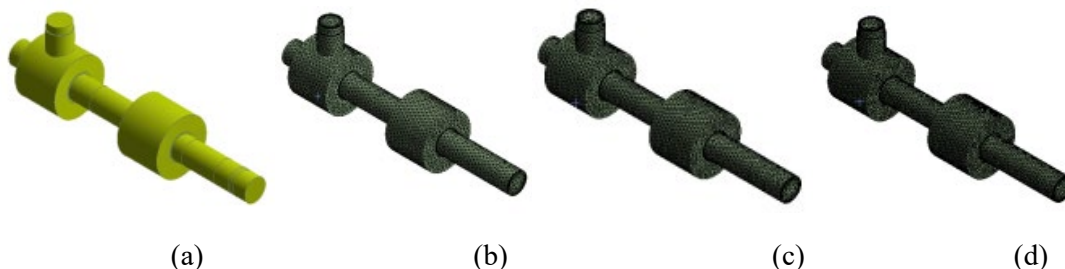
The pipe's model information such as the length and diameter were taken directly from the UTHM Biodiesel Plant. The model of the 3D pipe was taken from one of the pipes at the esterification process until the trans-esterification process and drawn using Solidwork. Figure 1 shows the assembly of the pipe model which consists of 13 parts.



**Figure 1: The assembly of the pipe model**

## 2.2 Grid generation

Grid generation is fundamental in numerical simulations, such as computational fluid dynamics (CFD) [17]. Grid is a form of foundation or preprocessing tool. In this research, the fluid domain for the pipe geometry is set before the mesh is run. The simulation's boundary is the fluid domain. The domain must contain all fluid components. The Figure 2 illustrates the fluid domain of the pipe geometry and the element size. The pipeline is then go through a meshing procedure with different element size (0.006 m, 0.007 m and 0.008 m). The three element size produce different element quantity which is 131601 elements, 90388 elements and 68318 elements respectively. Grid independence test, (GIT) were applied to the three element with different element quantity to evaluate the best grid for conducting the simulation analysis. The model with 90388 elements and 31992 nodes was chosen as the best element quantity.



**Figure 2: (a) Fluid domain and Grid generation (b) element size 0.008m (c) element size 0.007m (d) 0.006m**

## 2.3 Simulation study

Fluid-structure Interaction (FSI) were employed to simulate all instances in both fluid fluent and static structural simulations. A simulation experiment is a test or a set of tests in which significant modifications to the input variables of a simulation model are made in order to observe and understand the causes for changes in performance indicators [18].

### 2.3.1 Boundary condition for fluid flow simulation

The fluids Computational fluid dynamics (CFD) is a field of fluid mechanics that solves fluid flow problems using numerical analysis and algorithms. The computations necessary to model the interaction of liquids and gases with surfaces specified by boundary conditions are performed on high-performance computers. The Eq. 1, Eq. 2 and Eq. 3 shows the general equation

Reynolds Number,

$$Re = \frac{\rho v d}{\mu} \tag{Eq. 1}$$

Bernoulli equation (fluid flow head conservation),

$$Z_1 + \frac{\rho_1}{\rho_1 g} + \frac{v_1^2}{2g} = Z_2 + \frac{\rho_2}{\rho_2 g} + \frac{v_2^2}{2g} \tag{Eq. 2}$$

Viscosity,

$$\mu = \rho \nu \tag{Eq. 3}$$

The range of restrictions to boundary value issues in computational fluid dynamics is known as boundary conditions in fluid dynamics. Inlet boundary conditions, outlet boundary conditions, wall boundary conditions, and other boundary conditions are among them. Another need for transient issues is initial conditions, which provide the starting values of flow variables at nodes in the flow domain. Table 1 summarized the list of boundary conditions and other fluid properties used in the simulations.

**Table 1: Boundary condition and other fluid properties**

Parameter	Temperature (°C)					
	27			77		
Inlet pressure (kPa)	153	200	250	153	200	250
Outlet pressure (kPa)	88					
Fluid used	Biodiesel B100					
Viscosity $\mu$ (P)	$5.86e^{-3}$					
Density (kg/m <sup>3</sup> )	878					

### 2.3.2 Boundary condition for structure simulation

Young’s modulus is a measure of the ability of a material to withstand changes in length when under lengthwise tension or compression. Sometimes referred to as the modulus of elasticity, young’s modulus is equal to the longitudinal stress divided by the strain. Eq. 4 shows the formula for young modulus while Eq. 5 and Eq. 6 show Darcy’s head loss and shear stress formula respectively.

$$E = \frac{FL}{A\Delta L} \tag{Eq. 4}$$

Darcy’s Head Loss,

$$H_f = f \frac{L V^2}{D 2g} \tag{Eq. 5}$$

Shear Stress,

$$\tau = \mu \frac{d\gamma}{dt} \tag{Eq. 6}$$

The boundary conditions are the points at which the structure interacts, either by exerting external forces or by constraining motion. For this analysis, pressure from the fluid within the pipe was exerted to the wall of the pipe. Table 2 below show the Boundary condition in structure analysis.

**Table 2: Boundary condition in structure analysis**

Type of Pipe	Young Modulus, E (N/mm <sup>2</sup> )	Density (kg/m <sup>3</sup> )	Poisson Ratio
Stainless-steel	2E <sup>11</sup>	7850	0.3

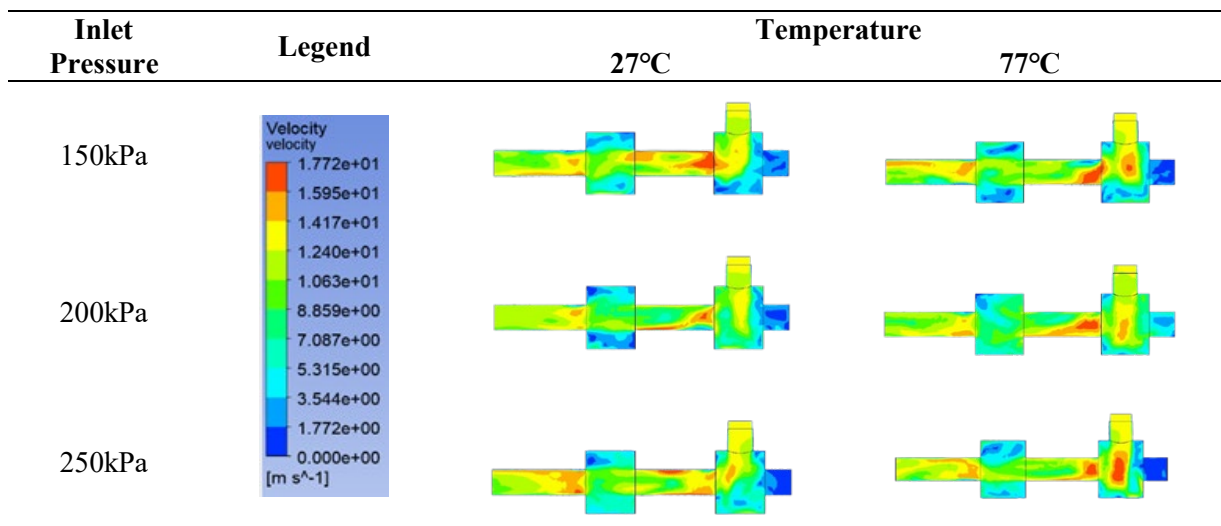
### 3. Results and Discussion

The flow behavior findings, such as velocity and pressure distribution along the pipe, the pipe's structural behavior, and performance, such as shear stress and stress distribution have been analyzed and discussed.

#### 3.1 Velocity distribution

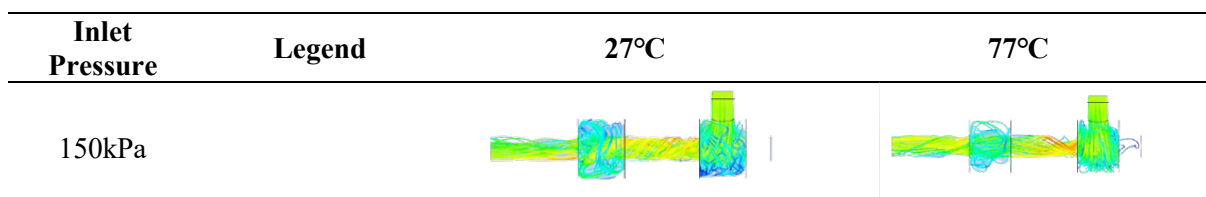
Table 3 below shows the velocity analysis inside the pipe model, which describes the contour of the velocity distribution along the pipe for each pressure inlet.

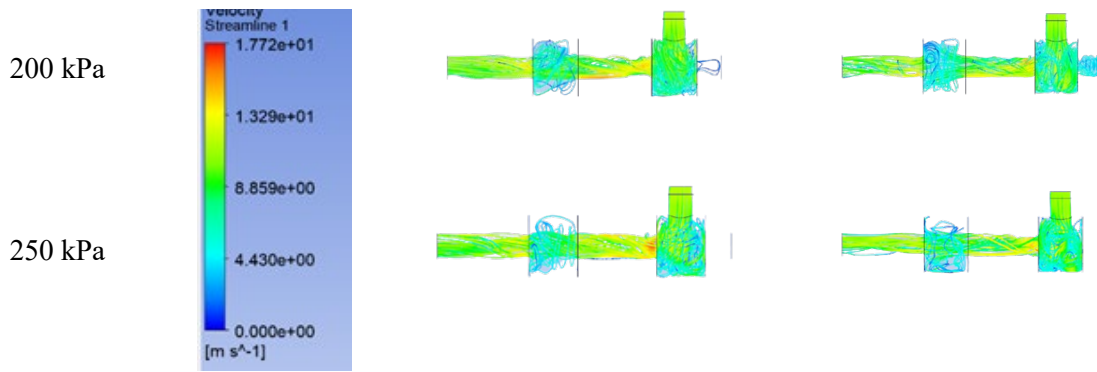
**Table 3: Velocity distribution in pipeline for two different fluid temperature**



For an inlet pressure of 153 kPa, the maximum velocity result for temperature 1 is higher than the maximum velocity result for temperature 2. The highest velocity in the pipe's fluid domain for temperature 1 is 9.49094 m/s, while the maximum velocity for temperature 2 is 9.29799 m/s. The maximum velocity in the fluid domain of the pipe at temperature 1 is 12.7895 m/s at an inlet pressure of 200kPa. The obtained velocity for model temperature 2 is 12.7876 m/s, which is a little drop. The maximum velocity of the fluid in the pipe at temperature 1 is 15.2161 m/s for the third inlet pressure of 250kPa. However, the maximum velocity measured for temperature 2 is a decrease of 14.9668 m/s. The result of Table 4 indicates that the inlet pressure and velocity are directly proportional. The velocity will increase as the inlet pressure is increased. Table 4 below tabulates the streamline of velocity for each inlet pressure and temperature.

**Table 4: Streamline of velocity in pipeline**





The results indicate that a transition occurs from laminar at the inlet, turbulent at the center of the pipe to laminar flow before it reaches the outlet. At even high velocity, the flow in the pipe's center becomes turbulent, with swirling streamlines across. Figure 3 below illustrates the velocity at the center of the pipeline for each inlet pressure in form of a graph.



**Figure 3: Velocity at Center of Pipeline**

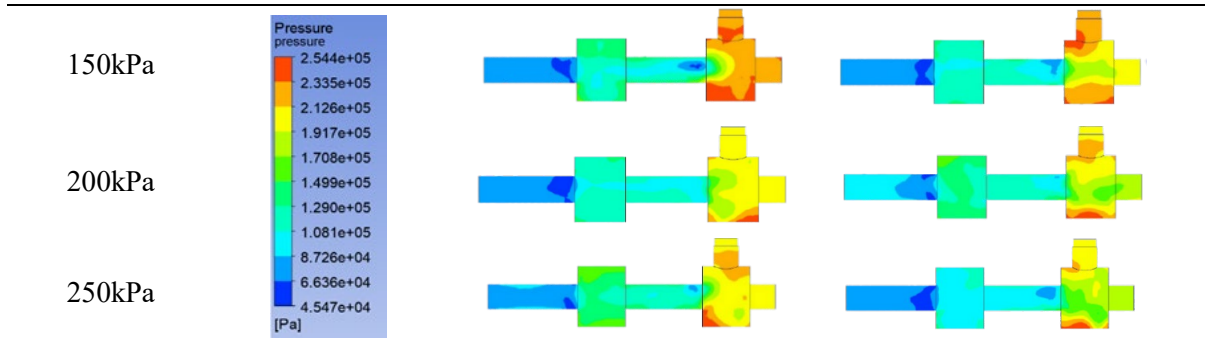
The highest velocity of fluid temperature 1 (27 °C) for inlet pressures of 153 kPa, 200 kPa, and 250 kPa is 9.36 m/s, 12.50 m/s, and 14.70m/s, respectively, according to the graph in Figure 3. While the peak value of fluid temperature 2 (77 °C) is 8.80 m/s for 153kPa, 11.30 m/s for 200 kPa, and 12.40 m/s for 250 kPa inlet pressure. The graph shows that the peak of fluid temperature 1 is higher than the peak of fluid temperature 2 in all three graphs. At distance 0m of the pipe, the velocity of fluid temperature 1 is also higher compared to fluid temperature 2 except for inlet pressure 200 kPa. At 0m of inlet pressure 250 kPa, the velocity of fluid temperature 2 is higher than fluid temperature 1.

### 3.2 Pressure distribution

Table 5 displays the pressure distribution analysis results for each inlet pressure and temperature by displaying the contour color that shows the maximum stress point. The comparison of pressure distribution contours across the pipe at various pressures is displayed.

**Table 5: Pressure distribution in pipeline for two different fluid temperature**

Inlet Pressure	Legend	27°C	77°C
----------------	--------	------	------



For all inlet pressures, the maximum pressure distribution result for temperature 2 is greater than the maximum pressure distribution result for temperature 1. The highest pressure in the pipe's fluid domain for temperature 1 is 141273 Pa, whereas the maximum pressure for temperature 2 is 142975 Pa at an inlet pressure of 153 kPa. At an inlet pressure of 200kPa, the maximum pressure in the fluid domain of the pipe at temperature 1 is 192448 Pa compared to the pressure recorded for model temperature 2 which is 193665 Pa. For a third inlet pressure of 250kPa, the maximum pressure of the fluid in the pipe at temperature 1 is 228280 Pa. The maximum pressure recorded for temperature 2 is 246715 Pa.

### 3.3 Structure behavior

Table 6 shows the results of the static non-uniform analysis for each geometry with a different inlet pressure and temperature. The contour color indicates the maximum stress position, which is utilized to assess distributions and determine structure longevity.

**Table 6: Von Mises equivalent stress**

Inlet Pressure	Legend	27°C	77°C
150 kPa			
200 kPa			
250 kPa			

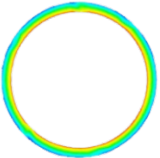
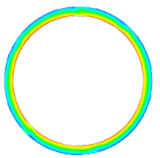
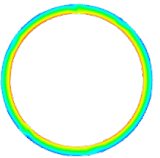
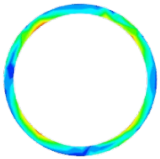
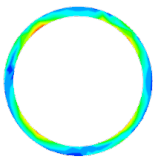
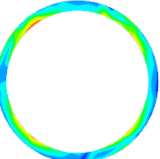
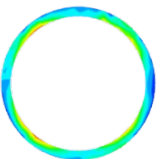
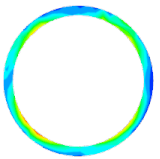
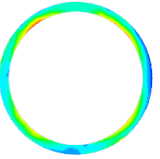

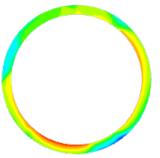
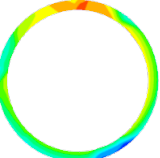
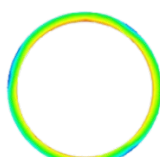
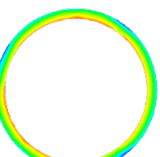
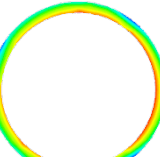
The maximum stress distribution result for temperature 1 is greater than the maximum stress distribution result for temperature 2 for all inlet pressures. At an inlet pressure of 153 kPa, the maximum stress on structure obtained for geometry temperature 1 is  $1.409 \times 10^7$  Pa, while the maximum stress value for geometry temperature 2 is  $1.29864 \times 10^7$  Pa. At an inlet pressure of 200 kPa, the pipe's maximum stress value at geometry temperature 1 is  $11.72101 \times 10^7$  Pa, while the stress value at geometry temperature 2 is  $11.54289 \times 10^7$  Pa. The maximum stress value of the pipe structure at temperature 1 is  $1.99118 \times 10^7$  Pa for a third inlet pressure of 250kPa. For geometry temperature 2, the

maximum stress value recorded is  $1.96813 \times 10^7$  Pa. According to the result, the maximal value of stress for input pressure is 250 kPa. Because when inlet pressure is increased, the stress distribution to the wall would also increase when contrasted with different inlet pressure.

### 3.4 Risk indicator

The risk indicator is built to evaluate the risks posed by the varying pressure inlets at each pipe fitting. The simulation software was used to obtain data for the maximum and minimum stress of the fitting. The data obtained is displayed as a cross-section at each fitting throughout the length of the pipe. The maximum and minimum stress at each fitting for each pressure inlet and temperature are shown in Tables 7 and Table 8.

**Table 7: Stress distribution along the fitting of the pipe at temperature 27 °C**

Fitting	153kPa	200kPa	250kPa
Fitting 1	 Min = 356.629kPa Max = 499.993kPa	 Min = 364.107kPa Max = 504.173kPa	 in = 367.967kPa Max = 516.697kPa
Fitting 2	 Min = 354.947kPa Max = 532.714kPa	 Min = 356.610kPa Max = 547.713kPa	 Min = 365.169kPa Max = 570.497kPa
Fitting 3	 Min = 327.459kPa Max = 509.972kPa	 Min = 328.113kPa Max = 520.148kPa	 Min = 283.756kPa Max = 479.446kPa
Fitting 4	 Min = 272.231kPa Max = 467.762kPa	 Min = 244.847kPa Max = 460.644kPa	 Min = 195.831kPa Max = 432.332kPa
Fitting 5	 Min = 271.521kPa Max = 573.922kPa	 Min = 300.123kPa Max = 620.445kPa	 Min = 341.447kPa Max = 703.123kPa



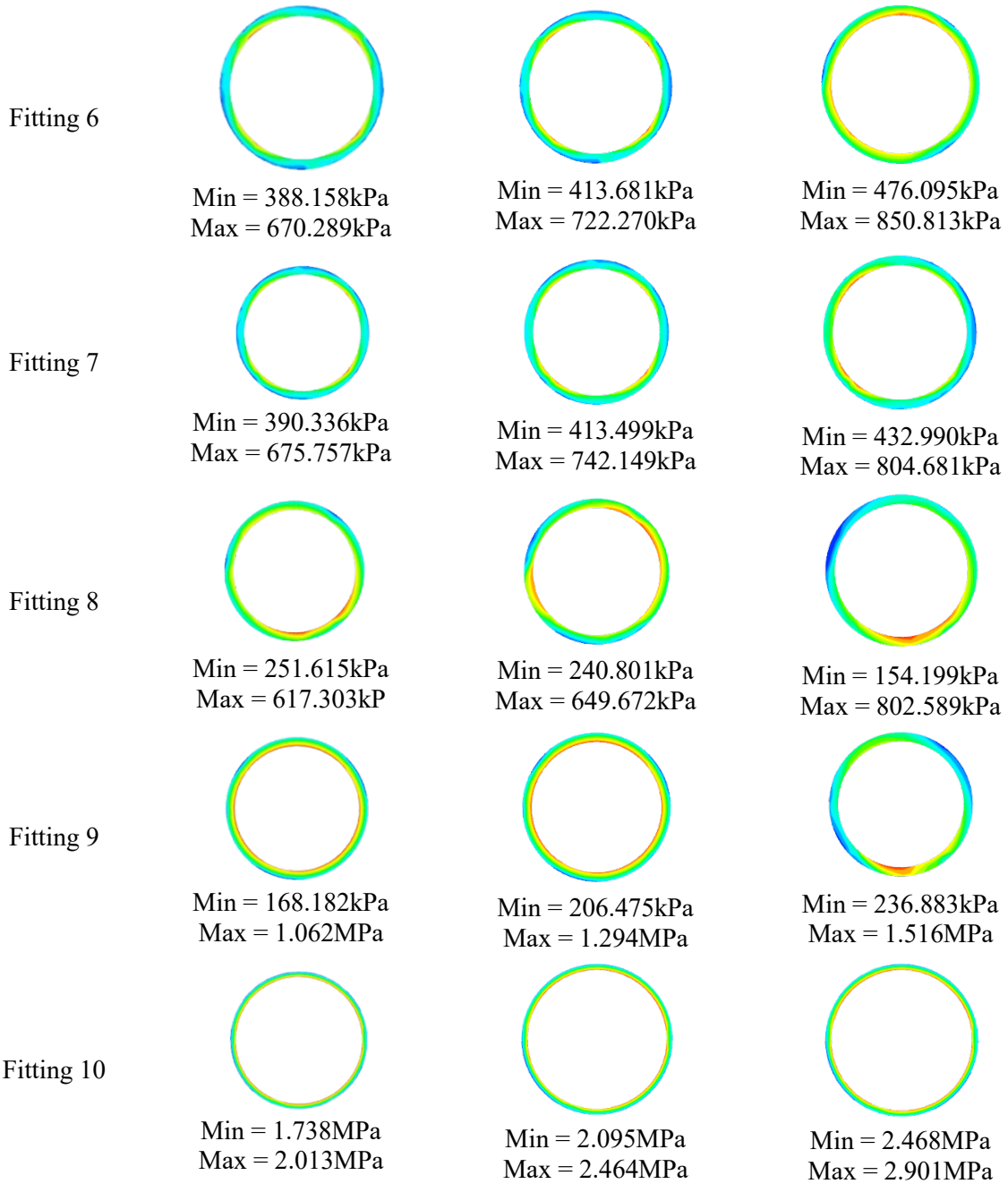
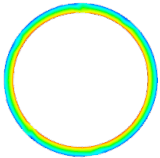
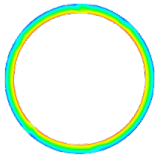
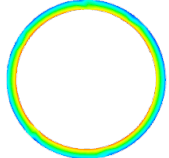
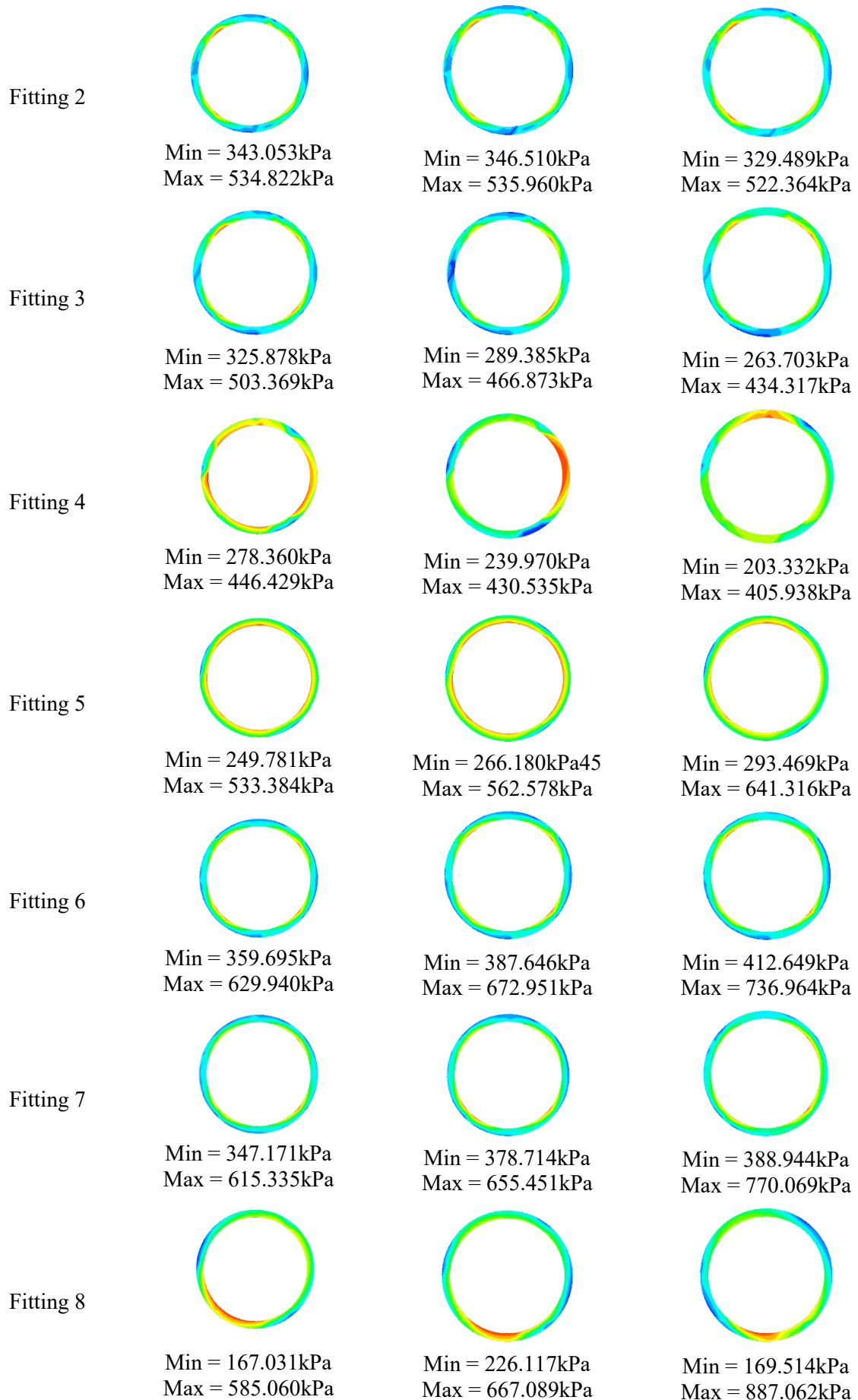
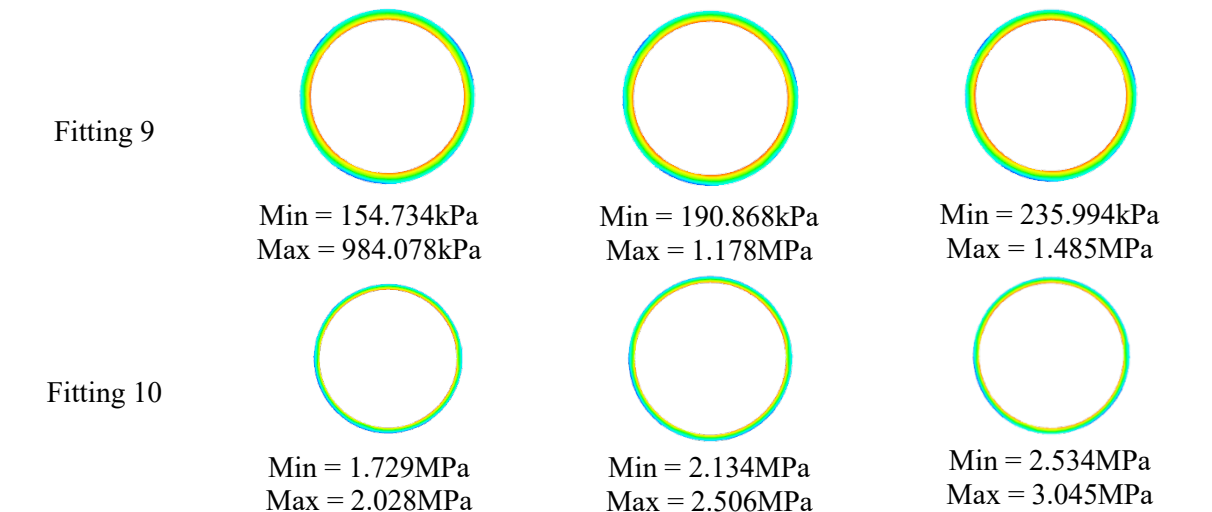


Table 8: Stress distribution along the fitting of the pipe at temperature 77 °C

Fitting	153kPa	200kPa	250kPa
Fitting 1	 Min = 359.395kPa Max = 495.496kPa	 Min = 357.149kPa Max = 493.746kPa	 Min = 354.353kPa Max = 492.432kPa





The stress distribution of three input pressures has a varied minimum and maximum value, as shown in Tables 7 and 8. It is related to the reason that the flow does not flow smoothly through the fitting in the pipe. There are variable stress values in each fitting. The minimum value of stress for all cases given is 7.823 Pa, while the maximum value is 3.099e5 Pa. According to this finding, the minimum value of stress for an inlet pressure of 153 kPa is 154.734 kPa at fitting 9, while the maximum value of stress is 2.028 MPa at fitting 10. At fitting 9, the lowest value of stress is 190.868 kPa for inlet pressure 200 kPa. At fitting 10, the maximum stress value obtained is 2.506 MPa. For an inlet pressure of 250 kPa, the minimum stress value is at fitting 8, which is 154.199 kPa, and the maximum stress value is at fitting 10, which is 3.045 MPa. This indicates that when the inlet pressure is high, the stress distribution to the wall will also increase compare to when the inlet pressure is low

#### 4. Conclusion

In conclusion, it can be determined that if the Biodiesel Plant operates at an inlet pressure of 250kPa, the risk of fitting 10 failing is greater than that of the other fitting. The comparison research discovered that when the temperature of the B100 rises, so would the flow inside the pipe. Furthermore, the input pressure affects the stress distribution on the pipe. As the inlet pressure rises, so will the stress distribution on the pipe. This is demonstrated by the simulation used in this study. It is suggested that the geometry be simplified based on the results of this investigation. The simplest recommendation possible, but also the hardest to implement.

#### Acknowledgement

The author thanks the Universiti Tun Hussein Onn Malaysia for offering a wide range of resources to acquire.

#### References

- [1] O. M. Ali, R. Mamat, C. K. M. Faizal, O. M. Ali, R. Mamat, and C. K. M. Faizal, "features Review of the effects of additives on biodiesel properties , performance , and emission features," vol. 012701, no. 2013, 2014, doi: 10.1063/1.4792846.
- [2] O. M. Ali, R. Mamat, N. R. Abdullah, and A. Adam, "Analysis of blended fuel properties and engine performance with palm biodiesel e diesel blended fuel," *Renew. Energy*, vol. 86, pp. 59–67, 2016, doi: 10.1016/j.renene.2015.07.103.
- [3] C. Q. Li, G. Fu, and W. Yang, "Stress intensity factors for inclined external surface cracks in pressurised pipes," *Eng. Fract. Mech.*, vol. 165, pp. 72–86, 2016, doi: 10.1016/j.engfracmech.2016.08.014.

- [4] F. Sundus, M. A. Fazal, and H. H. Masjuki, “crossmark,” *Renew. Sustain. Energy Rev.*, vol. 70, no. November 2016, pp. 399–412, 2017, doi: 10.1016/j.rser.2016.11.217.
- [5] L. C. Meher, D. V. Sagar, and S. N. Naik, “Technical aspects of biodiesel production by transesterification — a review,” vol. 10, pp. 248–268, 2006, doi: 10.1016/j.rser.2004.09.002.
- [6] Y. Chen, B. Huang, T. Chiang, and T. Tang, “Fuel properties of microalgae ( *Chlorella protothecoides* ) oil biodiesel and its blends with petroleum diesel,” *Fuel*, vol. 94, pp. 270–273, 2012, doi: 10.1016/j.fuel.2011.11.031.
- [7] S. Chongkhong, C. Tongurai, and P. Chetpattananondh, “Continuous esterification for biodiesel production from palm fatty acid distillate using economical process,” *Renew. Energy*, vol. 34, no. 4, pp. 1059–1063, 2009, doi: 10.1016/j.renene.2008.07.008.
- [8] D. Y. C. Leung, X. Wu, and M. K. H. Leung, “A review on biodiesel production using catalyzed transesterification,” *Appl. Energy*, vol. 87, no. 4, pp. 1083–1095, 2010, doi: 10.1016/j.apenergy.2009.10.006.
- [9] F. A. Zaher and H. M. Soliman, “Biodiesel production by direct esterification of fatty acids with propyl and butyl alcohols,” *Egypt. J. Pet.*, vol. 24, no. 4, pp. 439–443, 2015, doi: 10.1016/j.ejpe.2015.10.007.
- [10] J. Ding, Z. Xia, and J. Lu, “Esterification and Deacidification of a Waste Cooking Oil (TAN 68.81 mg KOH/g) for Biodiesel Production,” pp. 2683–2691, 2012, doi: 10.3390/en5082683.
- [11] H. Phan and A. S. Dhar, “Pipeline Maintenance Prioritization Considering Reliability and Risk : A Pipeline Maintenance Prioritization Considering Reliability and Risk : A Conceptual Methodology,” no. January, 2016, doi: 10.13140/RG.2.2.32088.55041.
- [12] M. Malek Mohammadi, M. Najafi, S. Kermanshachi, V. Kaushal, and R. Serajiantehrani, “Factors Influencing the Condition of Sewer Pipes: State-of-the-Art Review,” *J. Pipeline Syst. Eng. Pract.*, vol. 11, no. 4, p. 03120002, 2020, doi: 10.1061/(asce)ps.1949-1204.0000483.
- [13] S. Edora *et al.*, “Effect of Different Pipe Diameters to The Flow Behaviour of The Pipeline in UTHM Biodiesel,” vol. 1, no. 1, pp. 409–421, 2020.
- [14] G. W. Dzarma, A. Adeyemi, and A. Taj-liad, “EFFECT OF INNER SURFACE ROUGHNESS ON PRESSURE DROP IN A SMALL DIAMETER PIPE,” no. March, pp. 0–8, 2020.
- [15] R. Ahmad and S. Kamaruddin, “A review of condition-based maintenance decision-making,” *Eur. J. Ind. Eng.*, vol. 6, no. 5, pp. 519–541, 2012, doi: 10.1504/EJIE.2012.048854.
- [16] H. Iqbal, S. Tesfamariam, H. Haider, and R. Sadiq, “Inspection and maintenance of oil & gas pipelines: a review of policies,” *Struct. Infrastruct. Eng.*, vol. 13, no. 6, pp. 794–815, 2017, doi: 10.1080/15732479.2016.1187632.
- [17] C. A. Putra, “2-dimensional structured grid generation with smoothing , quality checking , and CFD data structure,” no. March, 2020.
- [18] A. Maria, “Introduction to modeling and simulation,” *Winter Simul. Conf. Proc.*, pp. 7–13, 1997, doi: 10.1145/268437.268440.